Design of Multi-Domain Joint Coding Scheme Based on Circular Mapping

W. X. Luo[1], Z. Chen[1]

[1]School of Mechanical Engineering and Electronic Information, China University of Geosciences, Wuhan 430074, China.

Corresponding author: Zhao Chen (chenzhao@cug.edu.cn)

Key Points:

- The joint encoding of space-time coding and direct sequence spread spectrum can greatly increase the reliability of communication systems.
- Circular mapping chaotic sequences as spreading codes can improve spreading performance.
- The joint simulation of LABVIEW and MATLAB/Simulink has been widely applied in the field of communication.

Abstract

With the rapid development of wireless communication technology and the increasing demand for communication quality in various fields, spread spectrum communication (SSC) and multiple input multiple output (MIMO) technology have become crucial research directions in the field of military communication, and space-time block coding (STBC) is an indispensable key technology in MIMO systems. This paper combined the excellent instrument interaction ability of LABVIEW and the data processing ability of MATLAB to build a direct sequence spread spectrum-space time block coding (DSSS-STBC) model based on circular mapping (CM) spread spectrum code, aiming at realizing multi-domain joint transmission of information in space, time, and power domains. The results demonstrated that the joint simulation platform of LABVIEW and MATLAB/Simulink successfully confirmed the superior spread spectrum performance of chaotic spreading codes based on circular mapping compared to traditional spreading codes. In addition, the multi-domain joint coding combining DSSS and STBC significantly enhanced the reliability and interference resistance of the communication system.

1 Introduction

In a wireless communication system, multiple input multiple output (MIMO) technology can effectively mitigate the fading of wireless channels and enhance the information rate of communication systems by utilizing multiple antennas for signal transmission and reception. MIMO technology stands out as a pivotal element in the fifth-generation mobile communication (5G), contributing to the reliability of wireless communication transmission through mechanisms such as diversity and multiplexing (Shi & Xiao, 2017; Sun, 2020; Yang & Sun, 2020). Operating without the need for additional spectral resources or increased antenna transmission power, MIMO technology optimally employs time, space, and frequency resources to elevate channel data throughput while minimizing transmission error rates. In order to obtain the maximum diversity and coding gain, space time block coding (STBC) technology is employed in signal transmission, achieving a synergistic combination of spatial and temporal dimensions (Wu et al., 2012; Feng et al., 2020; Mangla & Kumar, 2011). STBC achieves full diversity gain and low coding and decoding complexity (Bharti & Rawat, 2018). This paper utilizes the Alamouti coding techniques to achieve diversity, involving two pairs of receiving/transmitting antennas. However, in the context of the rapid evolution of communication technology, military communication must have stronger confidentiality and anti-interference. Spread spectrum technology has attracted extensive attention, and DSSS has been the most widely used spread spectrum method at present (Sajid et al., 2019). In military communication, there has been considerable research on common chaotic mappings in the context of spread spectrum technology. Due to the crucial importance of anti-interception and confidentiality in spread spectrum technology, continuous exploration of chaotic spread spectrum techniques is essential. Despite the prevalent use of circular mapping as a chaotic mapping in image encryption algorithms, it has not been investigated for its application in spread spectrum technology. Therefore, to further explore the capabilities of chaotic spread spectrum technology in military communication, this paper introduces the application of circular mapping in conjunction with direct sequence spread spectrum.

Reference (Qin et al., 2019) proposed a cyclic shift spread spectrum (CSSS) scheme for underwater acoustic (UWA) communication in multipath channels with long delays and severe Doppler frequency shifts. The receiver was able to mitigate co-channel interference by exploiting the periodic autocorrelation properties of the cyclically shifted spreading sequences. A new hybrid spread spectrum (HSS) technology in MIMO radar systems to protect the orthogonality of the transmitter and receiver was proposed (Chahrour et al., 2018), which could provide better narrow-band interference resistance. The spread spectrum enhancement technique proposed in literature (Yuchi et al., 2016) was based on traditional pseudo-random sequence and completely complementary sequence (CC-S), which could reduce the interference in MIMO systems. Literature (Quyen et al., 2017) proposed a DSSS communication system based on chaotic sequence, which adopted M-ary PSK modulation and combined with MIMO orthogonal frequency division multiplexing (OFDM) technology. This combination could improve the performance and capacity of traditional chaotic DSSS system. Literature (Cherni et al., 2011) introduced the performance optimization capability of spread spectrum sequences for code division multiple access (CDMA) MIMO systems, calculated the performance of a series of sequences and compared them with classical gold sequences to improve the performance of receivers.

Reference (Zhao et al., 2021) proposed a spread-spectrum code generation algorithm based on linear coupling of Sine mapping and Tent mapping, which significantly improved the complexity of mapping iterative generation of time series through a cascading approach, so that the generated spread-spectrum code had stronger pseudo-randomness. In reference (Wang et al., 2020), a signal simulation analysis system was established using MATLAB/Simulink to study the anti-interference performance of DSSS system based on logistic chaotic sequence. Experiments showed that the spread spectrum modulation of signals by chaotic spread spectrum sequence could effectively improve the anti-interference performance of signals. The DSSS and frequency-hopping spread spectrum (FHSS) (Hasjuks et al., 2022) were based on chaotic spread spectrum codes, which were compared with the classical M-sequence systems.

In view of the improvement of spread spectrum technology, the selection of spread spectrum codes holds particular significance for the performance of spread spectrum systems. In previous studies, the most common spread spectrum codes were m sequence and gold sequence. However, their periodicity limits the performance of spread spectrum, while chaotic mapping has good correlation and better randomness. Many studies have demonstrated that commonly used chaotic maps, such as logistic and Chebyshev, offer benefits including an extensive code set and robust anti-interference capabilities. Circular mapping chaotic sequences, frequently employed in neural networks and deep learning, have gained attention. Reference (Zhang et al., 2015) established a quantitative model for neural circuits based on the principles of circular mapping (CM) and symbolic dynamics. Meanwhile, Reference (Premnath et al., 2019) applied CM to image encryption, providing an evaluation of the effectiveness of CM and attractors in image encryption.

There has been insufficient exploration of circle mapping in the realm of spread spectrum technology. Therefore, this paper introduces a direct sequence spread spectrum method based on circular mapping. In addition, while STBC contributes to the reliability of the communication system, the combination of DSSS and STBC enables signal transmission across spatial, temporal, and power domains. Consequently, the CM-DSSS-STBC communication system enhances the anti-interference ability and maximize the diversity. The communication system in this paper is primarily implemented through the collaborative simulation platform of LABVIEW and Simulink. Although Simulink also utilizes a graphical language, its main strength lies in data processing when compared to LABVIEW. If this system is to be applied to NI virtual instruments in the future, LABVIEW is currently the optimal choice. Therefore, this paper employs a collaborative simulation platform using both LABVIEW and Simulink to realize the model.

2 CM-DSSS-STBC System

2.1 Circular mapping

Chaos refers to the unpredictable, random-like motion state of deterministic dynamical system that is highly sensitive to changes in the system's initial state. This definition emphasizes that the initial state of a chaotic system dictates its state at any given time. Because accurately describing the initial state of a chaotic system is challenging, and the motion of chaotic system is highly sensitive to the initial state, even a minor alteration in the starting state can result in a significant divergence in the system's state over time.

The CM is a chaotic map representing a mapping of the circle to itself. It is based on a nonlinear dynamical system, and generates a sequence of changes in a specified range by iteratively computing the input values. It is suitable for a variety of applications, including communication systems, cryptography, random number generation, and others. The complexity and randomness inherent in CM make the generated sequences exhibit favorable properties in certain applications. Nevertheless, in practical applications, it is necessary to pay attention to the selection and range limits of parameters, as well as possible convergence problems (Zhao et al., 2021; Wang et al., 2020; Zhang et al., 2015; Premnath et al., 2019).

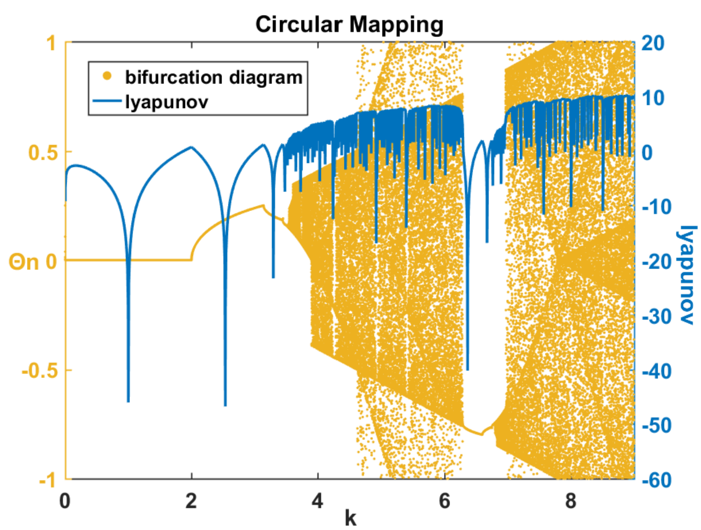

Figure 1. Bifurcation graph on the parameter space (0, k) of circular mapping and diagram of the relationship between Lyapunov exponent and k.

The most representative is the standard sinusoidal CM, such as Equations (1) and (2). When K is less than or equal to 1, it functions as a monotonic CM, resulting in periodic or quasi-periodic sequences. When K is bigger than 1, it is a non-monotonic circular map, and chaotic motion may occur in the supercritical region. Supercritical CM has complex bifurcation behavior. Fig. 16-1 in reference (Chen, 1998) delineates the bifurcation diagram of the parameter space of the standard CM. Fig. 1 illustrates the bifurcation diagram in the parameter space of the CM (0, K), indicating the commencement of chaotic states at a K value of approximately 3.55.

$$f_{\Omega}(\theta_n) = \theta_n + \Omega - \frac{K}{2\pi} sin(2\pi\theta_n) \quad (1)$$

$$\theta_{n+1} = mod(f_{\Omega}(\theta_n), 1) \quad (2)$$

When studying chaotic motion, the Lyapunov exponent is of utmost importance. It is one of the features used to identify several numerical values of chaotic motion, representing the numerical features of the average exponential divergence rate of adjacent trajectories in phase space. When K=2, period-doubling bifurcation occurs, and the critical point from period-doubling bifurcation to chaotic transition is 3.531. The process of period-doubling bifurcation acts as a pathway to chaos, representing a means of transitioning from a periodic window into chaos.

Circular mapping has the potential to substitute for pseudorandom code as spread spectrum code. As shown in Fig. 2, the chaotic sequence generated by the CM exhibits favorable autocorrelation and cross-correlation characteristics. The premise is that Ω and K values need to be selected in the chaotic region to generate the chaotic sequence. According to the bifurcation diagram of the parameter space of the CM before, Ω=0 and K=8.5 are selected in the model in this paper.

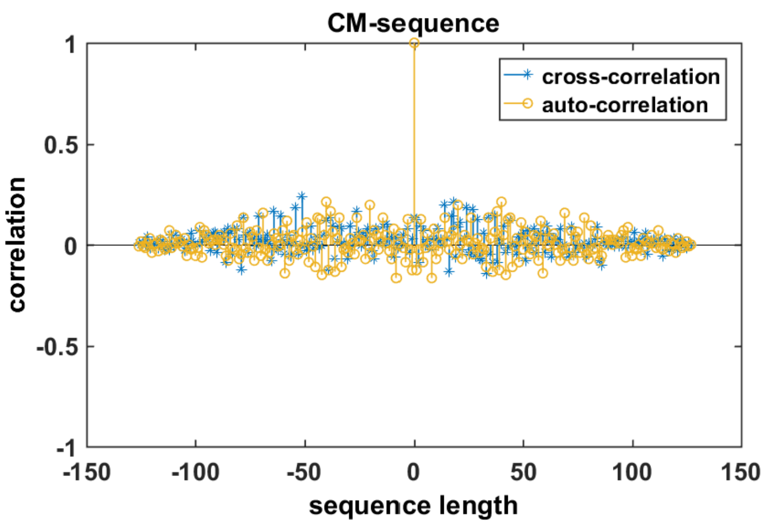

Figure 2. Auto-correlation and cross-correlation of circular mapping chaotic sequences.

2.2 Direct sequence spread spectrum

The Shannon formula indicates that channel capacity corresponds to the rate at which information is transmitted through the channel. Generally, a higher transmission rate is more advantageous for communication, making it crucial to enhance channel capacity. According to the Shannon formula, increasing signal bandwidth or improving signal-to-noise ratio can enhance channel capacity. Signal bandwidth is directly proportional to channel capacity, while signal-to-noise ratio is logarithmically proportional to channel capacity. Thus, it is evident that increasing signal bandwidth is more effective in enhancing channel capacity, and spread spectrum technology precisely increases the signal bandwidth. Consequently, spread spectrum technology could significantly boost channel capacity.

Furthermore, when the channel capacity remains constant, it is possible to reduce the communication system's requirement for signal-to-noise ratio by increasing signal bandwidth.

This implies that reliable information transmission can occur under low signal-to-noise ratio conditions by increasing signal bandwidth (Qin et al., 2019; Chahrour et al., 2018). Similarly, increasing signal-to-noise ratio can reduce the communication system's demand for signal bandwidth. This interchangeability between signal bandwidth and signal-to-noise ratio highlights the necessity of spread spectrum technology.

At present, the spread spectrum communication systems can be divided into three categories. The first is DSSS communication system, which directly extends the signal bandwidth through the spread spectrum code, allowing the communication system to establish reliable communication in the case of low SNR. The second is FHSS communication system, in which the carrier frequency is constantly hopping, and the frequency hopping is controlled by a pseudo-random sequence to ensure that it cannot be easily cracked by the enemy. The third is time-hopping spread spectrum (THSS) communication system. THSS means that the signal transmission time is jumping, and the transmitter uses a pseudo-random sequence to control whether the transmitter sends a signal in a certain period of time. Among the above (Yuchi et al., 2016; Quyen et al., 2017; Cherni et al., 2011), DSSS is the most widely used one, which is also the focus of this scheme.

The structure of the DSSS system is shown in Fig. 3. At the sending end, the raw data (bit sequence) is dot-multiplied by a ratio with the spread spectrum code. This introduces a higher frequency component into the signal, thus extending the spectrum of the signal. The spread spectrum code is a long sequence, usually pseudo-random, much longer than the original data. At the receiving end, the received extended signal is affected by noise and interference. To restore the original data, the receiver must have the same spread spectrum code. The receiver dot-multiplies the received signal with the spread spectrum code to shrink the spectrum of the signal again and recover the original data.

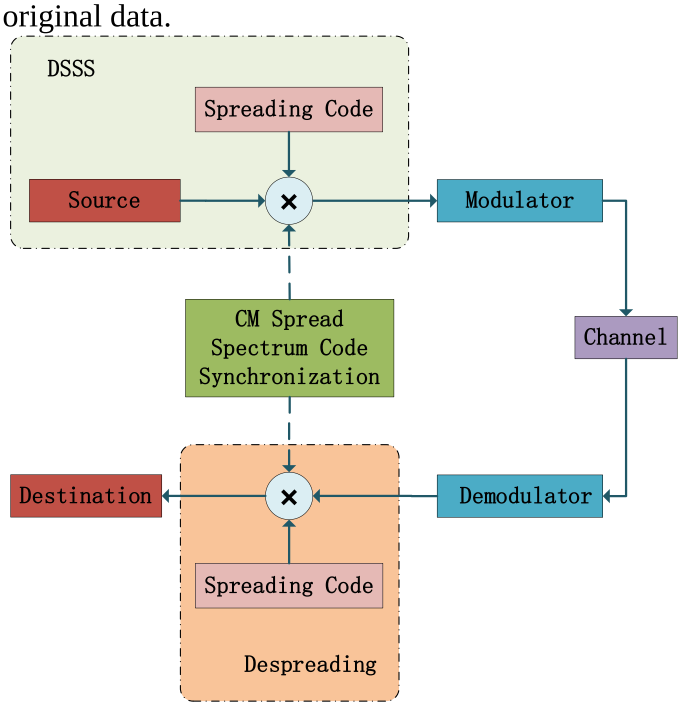

Figure 3. Block diagram of direct sequence spread spectrum system composition.

The spread spectrum code in the spread spectrum process plays a decisive role in the performance of the spread spectrum communication system. The selection of spread spectrum code requires attention to its good autocorrelation characteristics and the non-correlation between each spread spectrum code. The m-sequence is a kind of spread spectrum code that has been studied widely and applied. The term “m-sequence” is short for the longest linear feedback shift register sequence (Wang et al., 2020; Hasjuks et al., 2022). It is a pseudo-random sequence generated by a shift register with linear feedback. As a spread spectrum code, the m-sequence has many advantages, including good periodicity, superior autocorrelation, and good mutual correlation. Fig. 4 shows the auto-correlation and cross-correlation of m-sequence respectively.

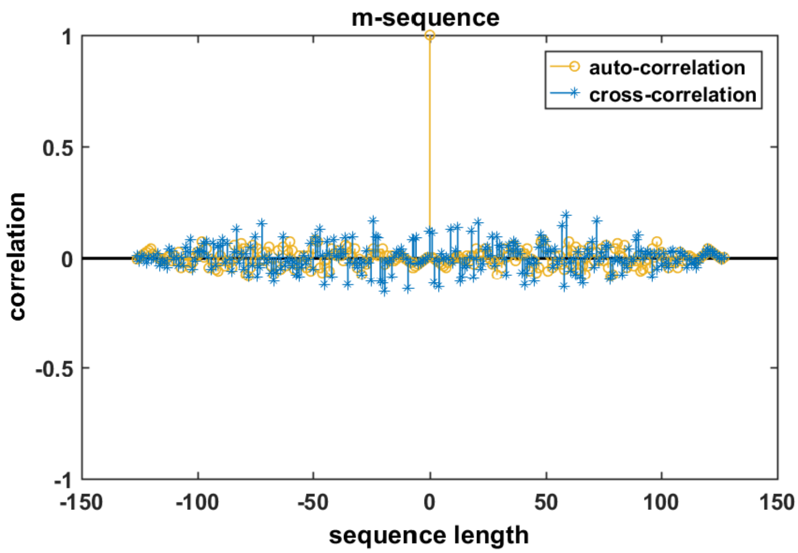

Figure 4. Auto-correlation and Cross-correlation of M-sequence.

2.3 Introduction to alamouti code principle

MIMO represents a breakthrough in wireless communication technology, doubling the capacity and spectrum utilization of the communication system without increasing bandwidth. It surpasses the Shannon capacity limit, enabling wireless transmission capacity to approach that of wired transmission. To approach the channel capacity of wireless MIMO systems in information transmission, researchers progressively extended the mature coding technology of single-input single-output (SISO) systems to MIMO systems, giving rise to space-time coding (Abed & Mohammed, 2019).

Rayleigh fading occurs when wireless signals propagate in complex wireless channels, and the fading characteristics differ in various spatial positions. If the distance between two positions exceeds the correlation distance between the antennas (typically more than 10 signal wavelengths apart), the two signals are considered entirely unrelated (Torabi & Haccoun, 2022; Mukhtar & Begh, 2022). Consequently, spatial diversity reception of signals can be achieved. Traditionally, diversity provides independent fading channels to receive multiple copies of the transmitted signal at the receiver and extract the transmitted signals from them. Since different bits of information fade independently, the probability that all copies fade deeply at the same time is very small, allowing the receiver to extract the sent bit from the received signal with minimal Rayleigh fading (Jang et al., 2019; Zhang et al., 2018).

Space-time codes are mainly divided into space-time trellis codes and space-time block codes. The received signal is detected by a maximum likelihood (ML) decoder. The earliest space-time coding is space-time trellis code (STTC). The number of diversities provided by STTC is equal to the number of transmitting antennas, and the coding gain depends on the complexity of code words without sacrificing bandwidth efficiency. While STBC can provide the same diversity gain as STTC, they lack coding gain. STBC is usually preferred because it requires only linear processing during decoding. In space-time coding technology, it is generally assumed that channel state information (CSI) is completely known at the receiver. When CSI is unknown at both ends, unitary space-time coding and differential space-time coding are proposed (Yu et al., 2010; Cuvelier et al., 2021).

STBC encodes a certain number of symbols output by the modulator in the wireless MIMO system into a space-time codeword matrix. A properly designed space-time block code can provide a certain degree of transmission diversity. STBC is usually completed by linear processing of input symbols in the complex number field. Therefore, leveraging this "linear" characteristic, a low complexity detection method can be employed to detect sending symbols.

This paper primarily investigates the implementation of Alamouti coding based on LABVIEW and MATLAB co-simulation, utilizing two transmitting antennas and two receiving antennas. The Alamouti coding scheme is a scheme is designed not to require CSI at the beginning. It encodes the transmitted symbols in both the space and time domains, making it an STBC structure. In this scheme, two consecutive symbols, x_1 and x_2, are coded according to the space-time codeword matrix of the following formula (3):

$$X = \begin{bmatrix} x_1 & -x_2^* \\ x_2 & x_1^* \end{bmatrix} \tag{3}$$

The Alamouti coded diversity gain is 2. Note that the diversity analysis is based on ML signal detection at the receiver (Hyeok & JUNG., 2020; Anusha & Rani, 2020). The ML signal detection for the Alamouti space-time encoding scheme is discussed below, assuming that the channel gains $h_1(t)$ and $h_2(t)$ remain the same in two consecutive symbol cycles:

$$\begin{aligned} h_1(t) = h_1(t+T_s) = h_1 = |\dot{h}_1|e^{j\theta_1} \\ h_2(t) = h_2(t+T_s) = h_2 = |h_2|e^{j\theta_2} \end{aligned} \tag{4}$$

Where $|\dot{h}_1|$ and θ_i represent the amplitude gain and phase rotation in two symbol cycles, and i=1,2. If y_1 and y_2 represent the received signals at t and $t+T_s$, then the received signals can be expressed as:

$$\begin{aligned} y_1 = h_1x_1 + h_2x_2 + z_1 \\ y_2 = -h_1x_2^* + h_2x_1^* + z_2 \end{aligned} \tag{5}$$

Where z_1 and z_2 represent the additive noise at t and $t+T_s$. The following matrix-vector expression is obtained by taking the complex conjugate of the second received signal:

$$\begin{bmatrix} y_1 \\ y_2^* \end{bmatrix} = \begin{bmatrix} h_1 & h_2 \\ h_2^* & -h_1^* \end{bmatrix} \begin{bmatrix} x_1 \\ x_2 \end{bmatrix} + \begin{bmatrix} z_1 \\ z_2^* \end{bmatrix} \tag{6}$$

The subsequent input-output relationships can be derived:

$$\begin{bmatrix} \tilde{y}_1 \\ \tilde{y}_2 \end{bmatrix} = (|h_1|^2 + |h_2|^2) \begin{bmatrix} x_1 \\ x_2 \end{bmatrix} + \begin{bmatrix} \tilde{z}_1 \\ \tilde{z}_2 \end{bmatrix} \tag{7}$$

From equation (7), it is evident that one antenna does not interfere with the other. In other words, the unwanted symbol x_2 is removed from y_1, and the unwanted symbol x_1 was removed from y_2. This elimination is a result of the complex orthogonality of the Alamouti code in equation (3). This property simplifies the structure of the ML receiver:

$$\hat{x}_{i,ML} = Q\left(\frac{\tilde{y}_i}{|h_1|^2+|h_2|^2}\right), i = 1 \quad (8)$$

3 Application of joint progamming in CM-DSSS-STBC

3.1 LABVIEW and MATLAB/Simulink hybrid programming method

The co-simulation of LABVEIW and MATLAB/Simulink has been widely applied in the field of communication. In this study, we employed the collaborative programming of LABVIEW and MATLAB/Simulink to further validate the communication performance of the DSSS-STBC communication system. MATLAB/Simulink excels in computing power and signal processing, surpassing most simulation platforms. However, it doesn't integrate well with hardware for real-time simulation. On the other hand, LABVIEW is adept at building virtual instruments through graphical language, making it convenient for real-time interaction with various test and measurement hardware, although it is less efficient in processing large amounts of data. Considering the strengths of both MATLAB/Simulink and LABVIEW, we constructed the communication system model in Simulink, performed data computation and signal processing in MATLAB, and, through collaborative programming, imported the data into LABVIEW. This joint programming method is conducive to the application of the communication simulation system in the interaction experiment between LABVIEW and instruments.

The integration of LABVIEW with MATLAB/Simulink is a significant approach in developing intelligent virtual instruments. Both LABVIEW and Simulink use graphical languages. In this study, the joint programming method was based on the dynamic link library (DLL) technology to achieve communication between the two software types. A DLL file, as an executable file, enables programs to share code and resources needed for special tasks (Peng & Zhu, 2007; Lv & Fu, 2010).

In the combined simulation environment of LABVIEW and MATLAB, the model interface toolkit (MIT) was essential. MIT supports more than 15 languages, including C/C++ and LABVIEW. It needed integration and packaging in NI VeriStand. The initial step involved building a simulation environment for NI VeriStand and MATLAB, associating VC++ and MATLAB before linking NI VeriStand and MATLAB. Once the environment was successfully established, the model in Simulink was compiled into a DLL file compatible with NI VeriStand. Finally, LABVIEW could call the DLL file through the model built by the MIT toolkit.

NI VeriStand is a software environment for configuring real-time test applications. It aids in configuring the real-time engine of multi-core processors for various tasks, such as analog, digital, communication bus and I/O interface based on field programmable gate array. NI VeriStand also supports tasks like triggering multi-file data recording, real-time incentive generation, computing channel, event warning, and early warning response programs. Importantly, NI VeriStand can import control algorithms, simulation models, and other tasks from NI LABVIEW software and third-party environments. The tasks are monitored and interacted with through a runtime editable user interface that incorporates numerous effective tools for mandatory assignments, alert monitoring, I/O calibration, and incentive configuration editing. Using NI VeriStand does not require programming knowledge, but it can be customized and extended in various software environments, including NI LabVIEW, American national standards institute (ANSI) C/C++, and other modeling and programming environments.

NI VeriStand real-time test applications typically encompass one or more real-time execution targets communicating with the host system via Ethernet. Each real-time execution target operates the NI VeriStand engine, configured through the Windows primary system, and deployed over Ethernet. Once the NI VeriStand engine configuration is deployed, interaction with the test system is possible at runtime using the NI VeriStand workspace window and the tools it provides, such as the incentive profile editor.

Additionally, joint programming of LABVIEW and MATLAB can be realized through the following methods:

MATLAB Script node: LabVIEW offers the MATLAB Script node to streamline the call process. It is worth noting that the MATLAB Script node has clear requirements on the type of input and output data. Data transmission can only be carried out if the data type in LabVIEW aligns with the data type in MATLAB.

ActiveX function template of LabVIEW: MATLAB supports ActiveX automation technology, treating MATLAB as an ActiveX server. The interface function provided by ActiveX interacts with MATLAB. The ActiveX channel is first established, and then the function or command is sent to MATLAB through the ActiveX channel. Subsequently, MATLAB executes it in the background.

Use dynamic data exchange (DDE) technology. DDE provides dynamic data exchange among programs running on the same computer or different computers. This technology has found extensive application in control software and information network integration due to its good real-time performance and easy network communication connection. Dynamic data exchange is based on Windows messaging mechanism, in which applications exchange information by conveying messages. Windows DDE uses client/server mode for messaging. The client serves as the requestor and receiver of data, while the server functions as the provider of data. The data transmission process involves three steps: request, reply and transmission (Huang, 2009).

3.2 Integrated model design for joint programming

The Simulink simulation model, as depicted in Fig. 5, illustrates a series of steps. First, the randomly generated binary number undergoes dot multiplication with the spread spectrum code, serving as a signal to extend the bandwidth of the original signal through DSSS. In a spread spectrum system, different spread spectrum gain can be obtained by changing the length of spread spectrum code. Subsequently, the signal the BPSK modulator block as a vector. The input vector is then subjected to orthogonal space-time coding to support both the time and space domains of orthogonal space-time block code (OSTBC) transmission. This coding scheme also includes an optional dimension, representing the frequency domain where encoding computations are independent. This dimension can be considered as the frequency domain. Given that there are 2 transmitting antennas, in each matrix, the entry (l,i) represents symbols sent from the ith antenna in the first time slot. The value of i ranges of 1 to 2, and the value of l spans from one to the total length of the code block.

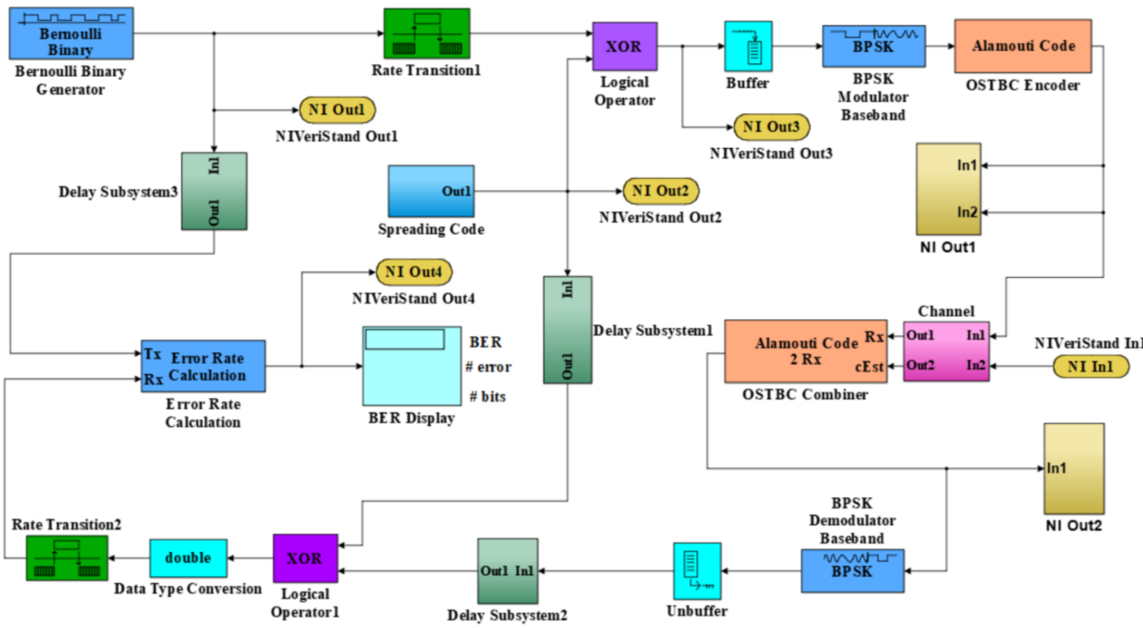

Figure 5. Simulation model for circular mapping multi domain joint coding based on Simulink.

After traversing the Rayleigh fading channel and Gaussian white noise channel, the signal undergoes joint decoding. The OSTBC combiner block amalgamates the input signal, derived from all receiving antennas, with the channel-estimated signal. This process aims to extract soft information concerning the symbols encoded through OSTBC. During the transmission of each codeword block, the input channel estimation may vary. In a MIMO communication system, a symbol demodulator or decoder follows the combiner block. This block conducts the combination operation for each symbol independently, and the decoding algorithm of this module is calculated according to the ML. After demodulation by BPSK, the signal needs to undergo dispreading. Pseudo-code synchronization is crucial, and this paper achieves it by connecting the same spread spectrum code module and incorporating a delay module. After synchronization, the signal is dot-multiplied with the spread spectrum code again to complete the signal dispreading. The model developed in this paper includes NI VeriStand Out before spread spectrum, after spread spectrum, after Alamouti encoder, and after Alamouti decoder. With these modules added, we can export output data or modify and set input data in LABVIEW.

After building the model in Simulink and running it successfully, proceed to convert the graphical model into a code file. During the actual code conversion process, there were occasional disruptions in the interface order. In essence, the Simulink input interface of the controller became disordered after DLL conversion. To avoid this error, it is crucial to verify the DLL input and output interfaces after each code conversion. The above is to complete the generation of the DLL file. It should be emphasized that generating a DLL file through Simulink was essentially the process of generating C or C++ code from the model, which can be used for embedded systems or hardware implementations, so a fixed-step solver must be used.

Fig. 6 shows the system simulation control Model built in LABVIEW. The "Model Path" function is used to input the path of simulation data file output from Simulink, and “Load

Model" loads the imported model into memory, preparing it for execution. This VI must be called to load the model before it can be executed in the control loop. "Model Period" outputs the running rate (in seconds) of the compiled model. A model is set to run at a certain rate, or step size, as defined in the build options when the model is compiled. However, the rate at which the Model Interface API actually steps the model is determined by how often the "Take Model Time Step" is executed in your application. The role of the "Take Model Time Step" is that write to model imports, run the model for one time step, and return values from outports. "NI In" and "NI Out" respectively correspond to the same module in Simulink.

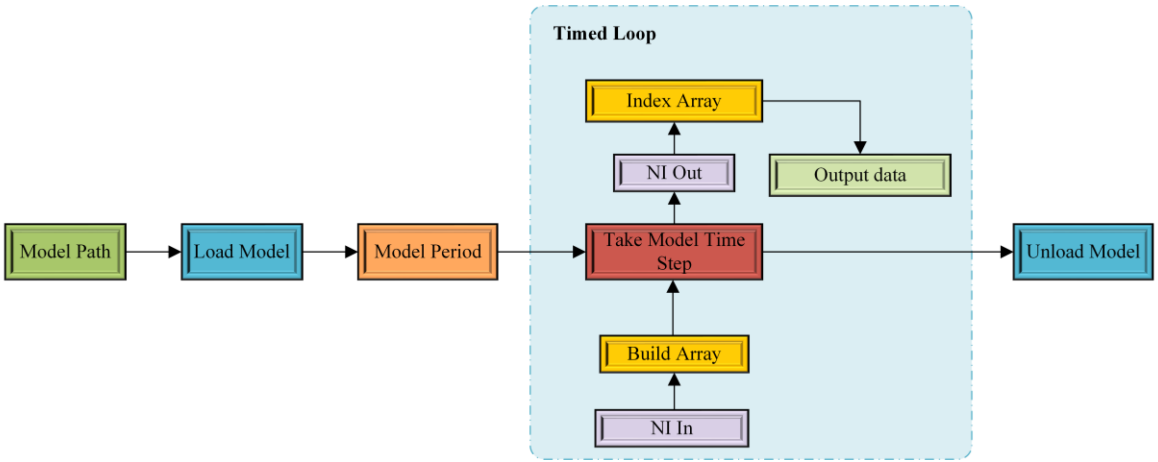

Figure 6. Simulation control system based on LABVIEW.

Fig. 7 illustrates the DSSS-STBC simulation model of joint programming designed in this paper. One part comprises the DSSS-STBC model based on Simulink, while the other part is the simulation control model based on LABVIEW. The two models exchange data through the NI interface. LABVIEW transmits the modified SNR Settings to the Simulink model through the NI interface. Simulink conveys signal processing in the simulation process to LABVIEW through NI interface, encompassing signal source, spread spectrum signal, Alamouti coded signal, Alamouti decoded signal, BPSK demodulation signal, and the BER of the entire Simulink model communication simulation process.

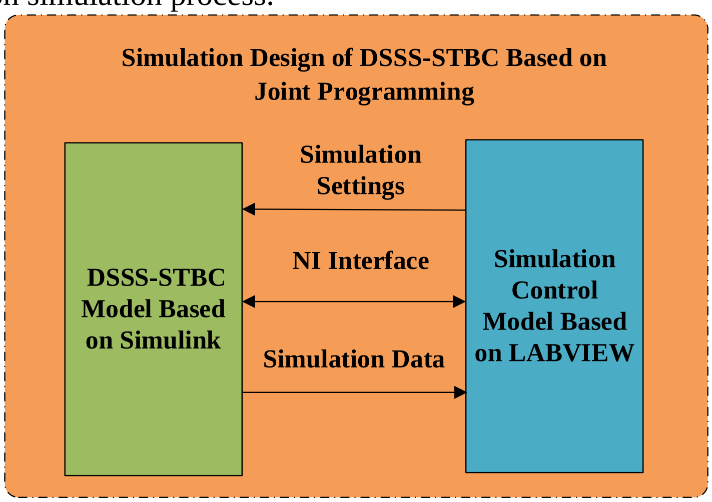

Figure 7. System composition diagram.

The output of the Simulink system model, denoted as $S[n]$, where n is the time index, is represented as follows in the data transmitted to LABVIEW:

$$L[n] = S[n] \tag{9}$$

Here, $L[n]$ is the signal passed to LABVIEW. This is a simplified description, and in reality, more details may be required, with the crucial aspect being the correct configuration of the data transfer interface between these two environments. The accuracy and abstraction level of the mathematical model depend on the model's purpose. In the context of this paper, the composite model is primarily implemented through the interface of the DLL file generated by Simulink and the calling operations in LabVIEW. This represents a high-level model, focusing on the system's components, interactions, and fundamental operations.

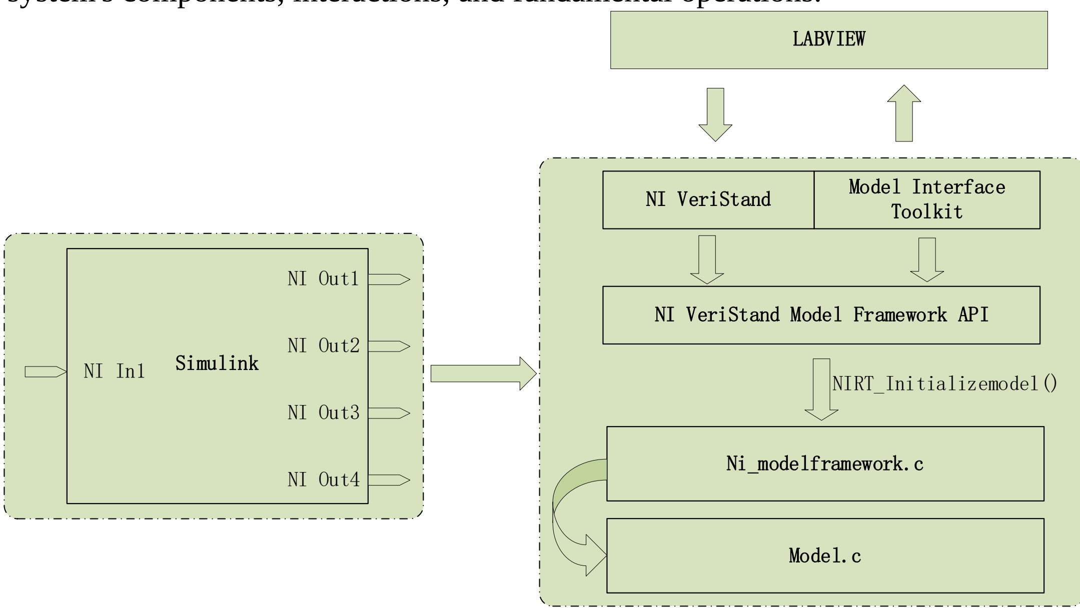

Figure 8. The model interaction diagram of the integrated system.

As shown in Figure 8, the model interaction diagram of the integrated system depicts the relationship between data input and output in the composite system. The NI interface in Simulink belongs to the NI VeriStand module. Therefore, the data, including NI In1, NI Out1, NI Out2, NI Out3, and NI Out4, output by Simulink will be shared with NI VeriStand and undergo processing. When running the NI VeriStand or Model Interface Toolkit test application, this application executes functions defined in the NI VeriStand model framework file. These function calls invoke functions in the model code, which, in turn, convert user-defined data types, initialize the model, and increment the time step in NI VeriStand. For instance, functions exported by the NI VeriStand model framework will call functions in the model code output by Simulink. During model execution, the test application can interact with the model by writing data to model inputs, reading data from model outputs, and adjusting model parameter values. LABVIEW can load and execute the model output from Simulink using the NI VeriStand model framework. LabVIEW VI models can be converted into compiled “lvmodel” files. Once the compiled “lvmodel” is deployed to the real-time target, NI VeriStand automatically copies the required DLL files to the target.

4 Experimental results

The LABVIEW-based simulation control model can modify and display Simulink models imported into LABVIEW in real time, and the total number of bits increases with continuously with the running time. As shown in Fig. 9, when comparing the bit error rates of Alamouti 2 × 2, Alamouti 2 × 1, and a single antenna transceiver, it can be clearly observed that performance of Alamouti 2 × 2 is the best. The comparison plot of the BER is derived from the BER calculation module in Simulink, which stores the output BER in the workspace and outputs its relation to SNR as an image.

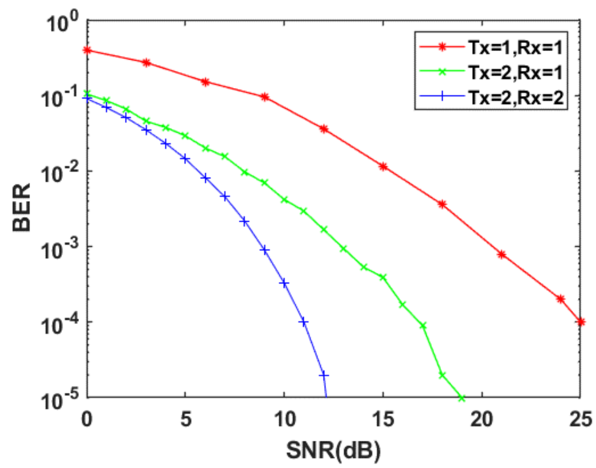

Figure 9. Comparison diagram of bit error rate of Alamouti coding.

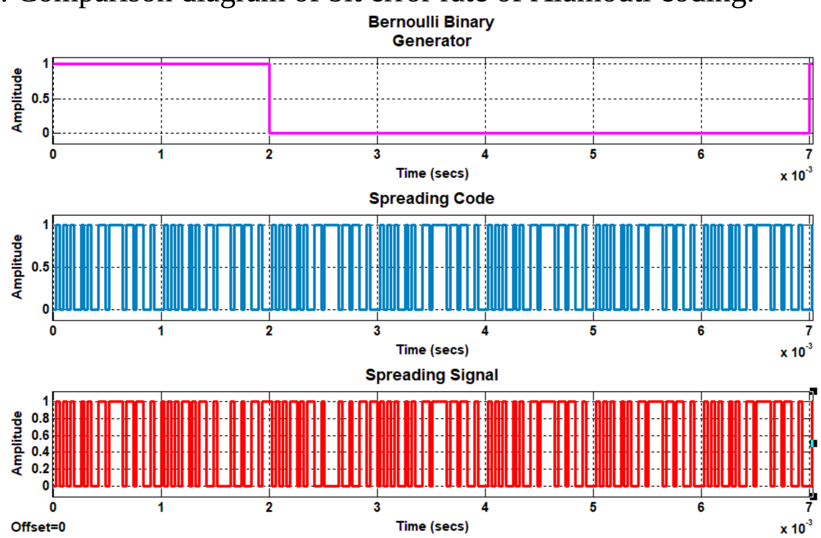

Figure 10. The time domain diagram of the spread spectrum code, the original signal and the signal after spread spectrum.

Fig. 10 illustrates the time domain diagram of the spread spectrum code, the original signal, and the signal after spread spectrum. The code rate of the original signal is 1kb/s, and the spread spectrum code has a code length of 31 bits with a rate of 31 kb/s. From the time-domain waveform, it is evident that the original signal became faster, and the symbol becomes narrower after the spread spectrum. In Fig. 11 and Fig. 12, the frequency domain diagrams of the original signal and the spread spectrum signal are presented. When the spread spectrum factor is 31, the signal bandwidth after spread spectrum extends by 31 times, and the signal spectrum after spread spectrum typically exhibits lower peak power because the signal energy is spread over a larger frequency band. The broadening of the spectrum implies that the signal is more evenly distributed across the frequency domain, and the energy of the signal is dispersed, facilitating easier signal transmission in interfered environments. The characteristic underscores one of the advantages of DSSS technology in terms of anti-jamming and anti-multipath fading.

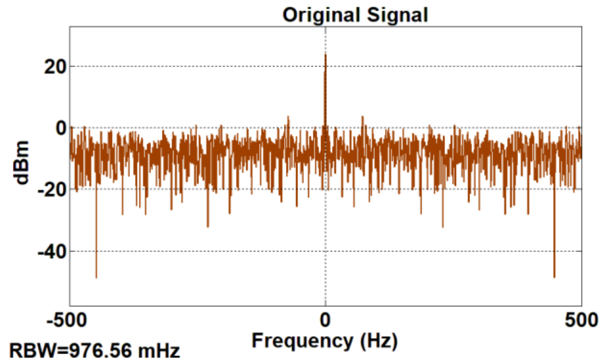

Figure 11. Original signal spectrum diagram.

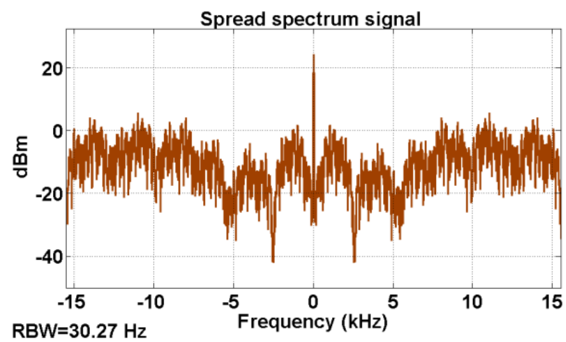

Figure 12. Spectrum diagram of spread spectrum signal.

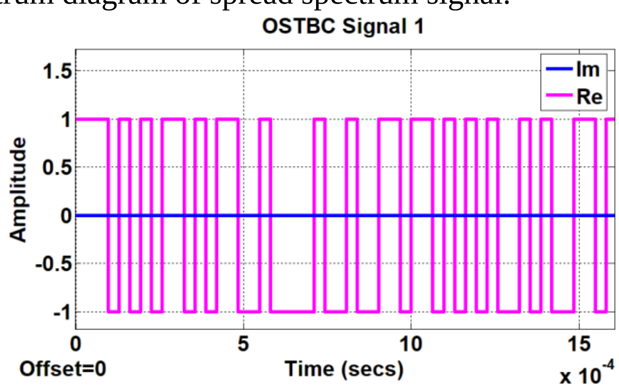

Figure 13. The signal transmitted by the first antenna in the Simulink model.

Fig. 13 and Fig. 14 display the signals transmitted by two antennas in the Simulink model respectively, encoded by Alamouti. Subsequently, these signals undergo filtering through a MIMO multipath fading channel, with the addition of Gaussian white noise. Upon reaching the receiver through the channel, Alamouti decoding is performed. The received signals are then combined, taking into account the channel estimate based on OSTBC. As shown in Fig. 15, the OSTBC Combiner block merges the input signal (from all receive antennas) with the channel estimate signal to extract soft information about the symbols encoded using OSTBC. It's noteworthy that the input channel estimate may vary during each codeword block transmission, and the combining algorithm uses only the estimate for the first symbol period per codeword block. A symbol demodulator or decoder would follow the Combiner block in a MIMO communications system, conducting the combination operation independently for each symbol.

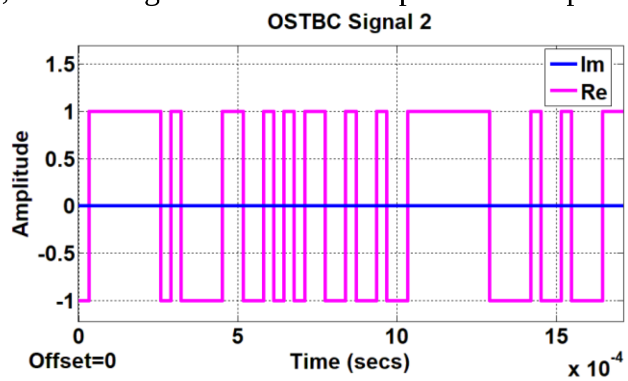

Figure 14. The signal transmitted by the second antenna in the Simulink model.

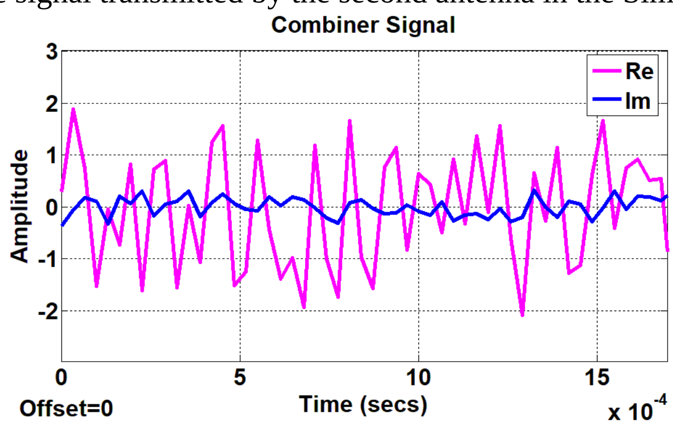

Figure 15. Alamouti decoded signal in the Simulink model.

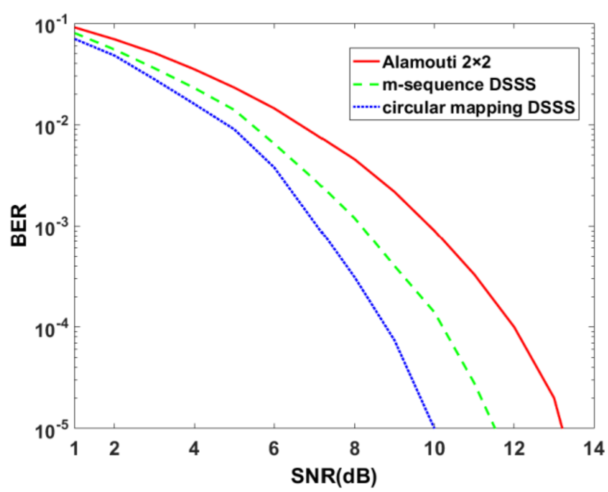

Figure 16. A comparison of the BER was made among the Alamouti 2 x 2 model without multi-domain joint coding, the DSSS-STBC system based on m-sequences, and the multi-domain joint coding communication system based on circular mapping.

As shown in Fig. 16, a comparison of the BER is conducted among the Alamouti 2 x 2 model without multi-domain joint coding, the DSSS-STBC system based on m-sequences, and the multi-domain joint coding communication system based on circular mapping. It can be observed that the communication performance of the multi-domain joint coding system based on circular mapping was superior. Fig.17 depicts the signal before and after spread spectrum, the output from the first transmitting antenna, the output from the second transmitting antenna, and the signal from Alamouti decoding output in the LABVIEW model. It can be seen that this paper successfully imported model data from Simulink into LABVIEW and is capable of real-time display and observation of the model data. Ultimately, it achieves the Alamouti encoding model based on the collaborative simulation of LABVIEW and Simulink.

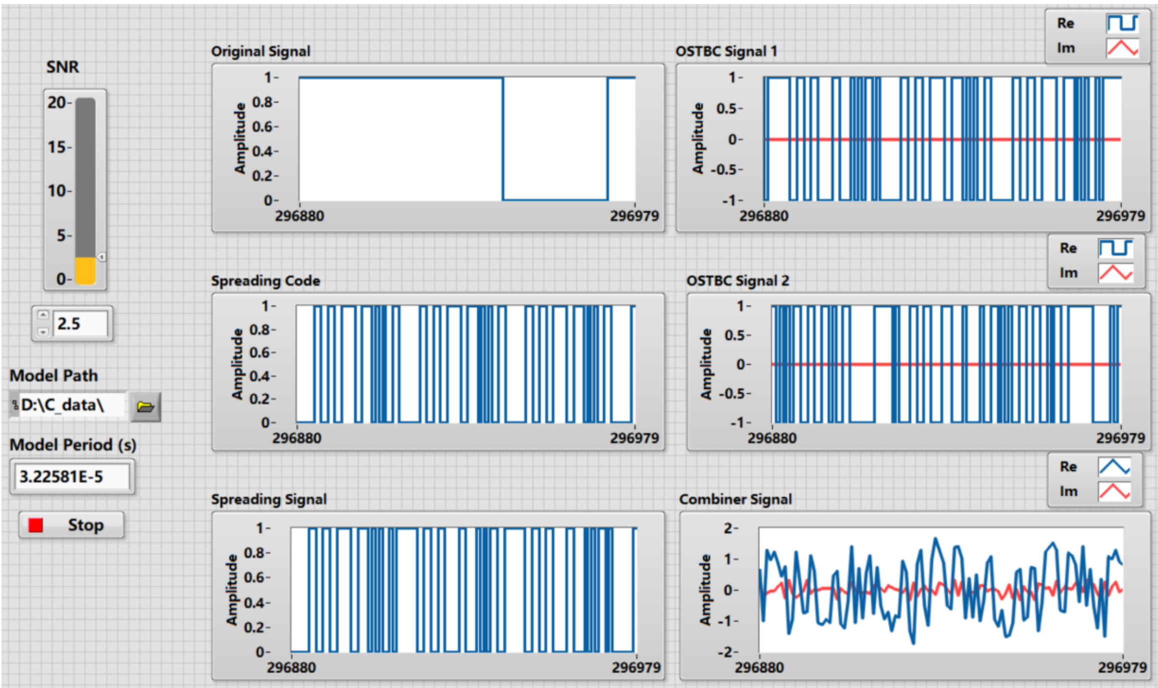

Figure 17. The signal transmitted by the first antenna in LABVIEW.

5 Conclusions

The multi-domain joint coding scheme based on circular mapping integrates DSSS with Alamouti coding, and convincingly demonstrates that the communication system can process signals through the time domain, space domain and power domain. Secondly, compared with the traditional pseudorandom sequence, the circle mapped chaotic sequence proves to be more suitable for spread spectrum communication, enhancing communication's resistance to interference. In this paper, the model is successfully built, and the signal is processed in Simulink. The code generated in Simulink is imported into the simulation control model in LABVIEW. The data interaction between the two platforms is successfully realized, verifying the correctness and integrity of the communication scheme. The co-simulation of LABVIEW and Simulink effectively promotes the application and expansion of DSSS-STBC technology. In subsequent research, the content of this paper holds significant reference value for the real-time interaction between the communication scheme and the instrument. Additionally, the multi-domain joint coding communication scheme based on circular mapping proposed in this paper contributes to the research on communication security and reliability in other fields.

Acknowledgments

This work was supported in part by the Research on Load Balancing of Space based UAV Cluster Edge Computing Network under Grant 62371429.

Open Research

Data were not used, nor created for this research.

References

Shi, X., & Xiao, B. (2017). Performance analysis of space-time coding in wireless communication. *Communications Technology*, *50*(12), 2670–2675.

Sun, H. N. (2020).Simulation study of Alamouti coding algorithm in MIMO system. *Journal of Changchun University of Engineering (Natural Science Edition)*, *21*(3), 51-55.

Yang, H., & Sun, L. (2022). MATLAB-based simulation of MIMO-OFDM communication system. *Computer Era*, *11*, 10-14+20. doi:10.16644/j.cnki.cn33-1094/tp.2022.11.003

Wu, J., Wu, X. B., Liu, T., & Sun, S. (2012). MATLAB simulation and FPGA implementation of Alamouti space-time packet code. *Video Engineering*, *36*(17), 73-75+95. doi:10.16280/j.videoe.2012.17.003

Feng, J., Liu, W., & Li, P. (2020). Design and implementation of MIMO communication system based on USRP platform. *International Electronic Elements*, *28*(18), 65-70+75. doi:10.14022/j.issn1674-6236.2020.18.015

Mangla, R., & Kumar, A. (2011). BER analysis of MIMO-OFDM wireless communication system with MATLAB Simulink. *International Journal of Applied Engineering Research*, *6*(23).

Bharti, P. K., & Rawat, P. (2018). Alamouti-STBC based performance estimation of multi Tx and Rx antenna over MIMO-OFDM. Paper presented at 2018 2nd International Conference on Trends in Electronics and Informatics (ICOEI), Tirunelveli, India.

Sajid, A., Habib, A., Ali, S., & Ejaz, S. (2019). Development of multi-user TDMA-based DSSS system. Paper presented at 2019 2nd International Conference on Communication, Computing and Digital systems (C-CODE), Islamabad, Pakista.

Qin, X., Qu, F., & Zheng, Y. R. (2019). Circular superposition spread-spectrum transmission for multiple-Input multiple-output underwater acoustic communications. *IEEE Communications Letters*, *23*(8), 1385-1388. doi: 10.1109/LCOMM.2019.2917192

Chahrour, H., Rajan, S., Dansereau, R., & Balaji, B. (2018). Hybrid spread spectrum orthogonal waveforms for MIMO radar. Paper presented at 2018 IEEE Radar Conference (RadarConf18), Oklahoma City, OK, USA.

Yuchi, Z., Shufeng, L., & Libiao, J. (2016). Application of MIMO enhancement technique based on spread spectrum method. Paper presented at 2016 IEEE International Conference on Electronic Information and Communication Technology (ICEICT), Harbin, China.

Quyen, N. X., Lam, N. T., Duy, D. H., Nguyen, N. P., & Vo, N. S. (2017). Chaos-based spread-spectrum using M-ary PSK and OFDM-MIMO. Paper presented at 2017 International Conference on Recent Advances in Signal Processing, Telecommunications & Computing (SigTelCom), Da Nang, Vietnam.

Cherni, A., Jemaa, Z. B., & Belghith, S. (2011). Performance of conventional receiver in a CDMA MIMO system using non classical spread spectrum sequences. Paper presented at 2011 International Conference on Communications, Computing and Control Applications (CCCA), Hammamet, Tunisia.

Zhao, L., Bao, L. Y., & Ding, H. W. (2021). S-T linearly coupled cascaded chaotic spread spectrum codes and their performance analysis. *Telecommunication Engineering*, *61*(2), 218-223.

Wang, S. Y., Yu, Q. F.,& Ou, P. (2020). Simulation analysis of anti-interference in direct spread spectrum systems based on chaotic sequences. *Network Security Technology & Application*, 12, 53-55.

Hasjuks, N., Hellbruck, H., & Aboltins, A. (2022). Performance study of chaos-based DSSS and FHSS multi-user communication systems. Paper presented at 2022 Workshop on Microwave Theory and Techniques in Wireless Communications (MTTW), Riga, Latvia.

Zhang, H., Ding, J., & Tong, Q. Y. (2015). A study on the neural information processing mechanism for determining the direction of sound sources based on the amplitude difference between the two ears. *Acta Physica Sinica*, *64*(18), 474-480.

Premnath, R., Arumugham, S., Rethinam, S., Lakshmi, C., & Rengarajan, A. (2019). Performance evaluation of chaotic maps & attractors in image encryption. Paper presented at 2019 International Conference on Computer Communication and Informatics (ICCCI), Coimbatore, India.

Chen, S. G. (1998). Circle maps (pp. 71-76). China: Shanghai Science and Technology Education Press.

Abed, W. M., & Mohammed, R. K. (2019). Investigating the performance of various channel estimation techniques for MIMO-OFDM systems using matlab. *SSRN Electronic Journal*, *9*(5). doi:10.2139/ssrn.3486124

Mujeeb, S. S., & Jyothsna, M. (2021). Implementation of MIMO-OFDM system using V-BLAST ZF and V-BLAST MMSE detection algorithms. *Materials Today : Proceedings*. doi: 10.1016/j.matpr.2020.11.542

Torabi, M., & Haccoun, D. (2022). Physical layer secrecy of a cognitive radio with spatially correlated alamouti ostbc system. *Physical Communication*.

Mukhtar, S., & Begh, G. R.. (2022). Error analysis of tas-ostbc assisted downlink noma system over generalized η-μ fading channel. *International Journal of Communication Systems*, *35*(13).

Jang, D. S., Jeong, U. S., Ryu, G. H., & Kyunbyoung, K. O. (2019). On ber analysis and comparison for ostbc mimo df relaying networks. *IEICE Transactions on Fundamentals of Electronics Communications and Computer Sciences*, *E102.A*(6), 825-833. doi: 10.1587/transfun.E102.A.825

Zhang, D. M. Wang, Y. F., Cha, F. C., & Zhou, J. (2018). Design of spatial modulation scheme for superimposed space-time packet codes. *Journal of Nanjing University of Posts and Telecommunications (Natural Science Edition)*, *38*(2), 8-13+21. doi:10.14132/j.cnki.1673-5439.2018.02.002

Yu, L. N., Wang, Y., & Gao, K. (2010). Simulation and analysis of quasi-orthogonal space-time packet code performance. *Informatization Research*, *36*(1), 19-21. doi:10.3969/j.issn.1674-4888.2010.01.006.

Cuvelier, T. C., Lanham, S. A., Cour, L. B. R., & Heath, R. W. (2021). Quantum codes in classical communication: a space-time block code from quantum error correction. *IEEE Open Journal of the Communications Society*, 2, 2383-2412. doi: 10.1109/OJCOMS.2021.3121183

Hyeok, Koo, & JUNG. (2020). Sign reversal channel switching method in space-time block code for ofdm systems. *IEICE Transactions on Fundamentals of Electronics, Communications and Computer Sciences*, *E103.A*(2), 567-570. doi:10.1587/transfun.2019EAL2090

Anusha, M. K., & Rani, S. C. (2020). Improvement of FER using differential space-time block code. *International Journal of Recent Technology and Engineering (IJRTE)*, *8*(5), 4144-4148.

Peng, Y. N., & Zhu, H. (2007). Using DLL technology to realize LabVIEW and MATLAB hybrid programming. *Computer and Modernization*, 8, 93-95.

Lv, P. P., & Fu, Q. (2010). Application of LabVIEW and matlab in radar signal simulation. *Fire Control Radar Technology*, *39*,(2), 45-48. doi:10.19472/j.cnki.1008-8652.2010.02.010

Huang, S. K., Peng, Y. N., Xie, S. P., & Wei, D. H. (2009). Hybrid programming method and application of LabVIEW and Matlab/Simulink. *Research and Exploration in Laboratory*, *28*(7), 67-71.